

Supplementary Information

Amorphous MOF Conversion Strategy for Membrane Fabrication with Unique Surface Architecture

Zilun Guo,^a Hiroto Maruta^a and Shunsuke Tanaka^{*bcd}

- a Graduate School of Science and Engineering, Kansai University, 3-3-35 Yamate-cho, Suita-shi, Osaka 564-8680, Japan.
- b Department of Chemical, Energy, and Environmental Engineering, Faculty of Environmental and Urban Engineering, Kansai University, 3-3-35 Yamate-cho, Suita-shi, Osaka 564-8680, Japan.
- c Organization for Research and Development of Innovative Science and Technology (ORDIST), Kansai University, 3-3-35 Yamate-cho, Suita-shi, Osaka 564-8680, Japan.
- d Carbon Neutrality Research Center (CNRC), Kansai University, 3-3-35 Yamate-cho, Suita-shi, Osaka 564-8680, Japan.

*E-mail: shun_tnk@kansai-u.ac.jp

Table of Contents

	Pages
Materials and Methods	S2
Preparation of Zn–Hmim Network Precursor Solution (<i>amp</i> -Zn–Hmim Sol)	S2
Synthesis of <i>amp</i> -Zn–Hmim/AAO Membranes	S2
Vapor-Induced Crystallization: Preparation of ZIF-8/AAO Membranes	S2
Characterization	S3
Fig. S1 Amorphous Zn–Hmim solution using different solvent amount.	S4
Fig. S2 FTIR spectrum of <i>amp</i> -Zn–Hmim.	S5
Fig. S3 XRD patterns of membranes.	S6
Fig. S4 Single-gas permeation characteristics.	S7
Fig. S5 N ₂ adsorption and desorption isotherms.	S8
Fig. S6 FESEM images of AAO substrate.	S9
Fig. S7 FESEM image of concave-defected ZIF-8 crystals.	S10
Fig. S8 Comparison of the gas permeation characteristics.	S11

Materials

All commercially available chemicals were used as received without further purification. Zinc acetate dihydrate ($\text{Zn}(\text{OAc})_2 \cdot 2\text{H}_2\text{O}$, $\geq 99.0\%$), zinc nitrate hexahydrate ($\text{Zn}(\text{NO}_3)_2 \cdot 6\text{H}_2\text{O}$, $\geq 99.0\%$), and 2-methylimidazole (Hmim, $\text{C}_4\text{H}_6\text{N}_2$, $\geq 99.0\%$) were purchased from FUJIFILM Wako Pure Chemical Industries. Methanol ($\geq 99.8\%$), ethanol ($\geq 99.5\%$), 1-butanol ($\geq 99.0\%$), *N,N*-dimethylformamide (DMF, $\geq 99.5\%$), and *N*-methylformamide (NMF, $\geq 99.0\%$) were obtained from Sigma-Aldrich. Anodic aluminum oxide membranes (AAO, AnodiscTM47, pore diameter: 20 nm, thickness: 60 μm , diameter: 47 mm) were purchased from WhatmanTM.

Preparation of Zn–Hmim Network Precursor Solution (*amp*-Zn–Hmim Sol)

Zinc acetate dihydrate (2.50 mmol) and 2-methylimidazole (5.00 mmol) were dissolved in a fixed amount of solvent, maintaining a Zn : Hmim molar ratio of 1 : 2. Several solvents (methanol, ethanol, 1-butanol, DMF and NMF) were screened, and 1-butanol was selected for membrane preparation. The solution was then left to stand at room temperature for one week to form the amorphous Zn–Hmim (*amp*-Zn–Hmim) network. The resulting clear solution was used as the *amp*-Zn–Hmim precursor solution for subsequent membrane fabrication.

Synthesis of *amp*-Zn–Hmim/AAO Membranes

A volume of 0.2 mL of the *amp*-Zn–Hmim precursor solution was dropped onto the surface of an AAO support and spin-coated under fixed conditions (3000 rpm, 30 s) to obtain the *amp*-Zn–Hmim/AAO membrane.

Vapor-Induced Crystallization: Preparation of ZIF-8/AAO Membranes

The crystalline ZIF-8/AAO membrane was prepared via vapor-induced crystallization of the *amp*-Zn–Hmim/AAO membrane. The as-prepared *amp*-Zn–Hmim/AAO membrane and 1-butanol (20 mL) were placed separately in a sealed perfluoroalkoxy (PFA) container, ensuring no direct contact between the membrane and the liquid solvent. The sealed container was then heated in an oven at 130 °C for a specified period, allowing 1-butanol vapor to induce crystallization of the *amp*-Zn–Hmim into the ZIF-8 framework. Following vapor treatment, the membrane was further heated at 140 °C to remove residual impurities, including acetic acid originating from the zinc acetate precursor and remaining 1-butanol. The resulting crystalline membrane was designated as ZIF-8/AAO and used for subsequent characterization and gas permeation measurements.

Characterization

Powder X-ray diffraction (PXRD) was performed at room temperature under atmospheric pressure using a RIGAKU MiniFlex600. CuK α ($\lambda = 1.5418 \text{ \AA}$) was used as an X-ray tube at 30 kV and 15 mA.

Pair distribution function (PDF) measurements were performed at the BL13XU beamline of SPring-8, Japan. High-energy X-ray with an energy of 35 keV ($\lambda = 0.354384 \text{ \AA}$) was used to obtain total scattering data suitable for PDF analysis. Samples were loaded into borosilicate glass capillaries (inner diameter: 0.5 mm). The exposure time was adjusted to ensure sufficient signal-to-noise ratio while avoiding detector saturation. Real-space refinements were carried out using PDFgui, where the experimental $G(r)$ was fitted to structural models to determine local atomic arrangements.

Thermogravimetric analysis (TGA) was conducted using a Shimadzu Corporation DTG-60H. The BET area and pore volume were obtained by performing N₂ adsorption/desorption measurements at 77 K using a MicrotracBEL BELSORP-max. Before adsorption measurements, pre-treatment was performed by heating at 225°C for 4 h in a vacuum using a MicrotracBEL BELPREP-vac.

Field emission scanning electron microscope (FESEM) images were recorded on a Hitachi High-Tech S-4800. The measurement was performed at an acceleration voltage of 1.0 to 3.0 kV and an emission current of 10 μA .

The obtained membrane was mounted in a pressure-type gas permeation cell operated using the differential pressure method, and single-component gas permeation tests were conducted. The feed pressure was maintained at 100 kPa, and the test gases used were H₂, CO₂, N₂, CH₄, C₃H₆ and C₃H₈. The cell temperature was kept at 35°C. The obtained permeance values were converted to the standard unit, the gas permeation unit (GPU), where $1 \text{ GPU} = 3.35 \times 10^{-10} \text{ mol/m}^2 \cdot \text{s} \cdot \text{Pa}$. Furthermore, the ideal separation factor was calculated from the ratio of the permeances of each gas pair.

X [mmol]	zinc acetate						zinc nitrate	
	10	20	50	100	300	500	1000	10
DI water								
Methanol								
Ethanol							—	
1-butanol							—	
DMF				—	—	—	—	—
NMP				—	—	—	—	—

Fig. S1 Synthesis of amorphous Zn–Hmim solution using different solvent amounts (Zn : Hmim : solvent = 0.25 : 0.5 : X mmol).

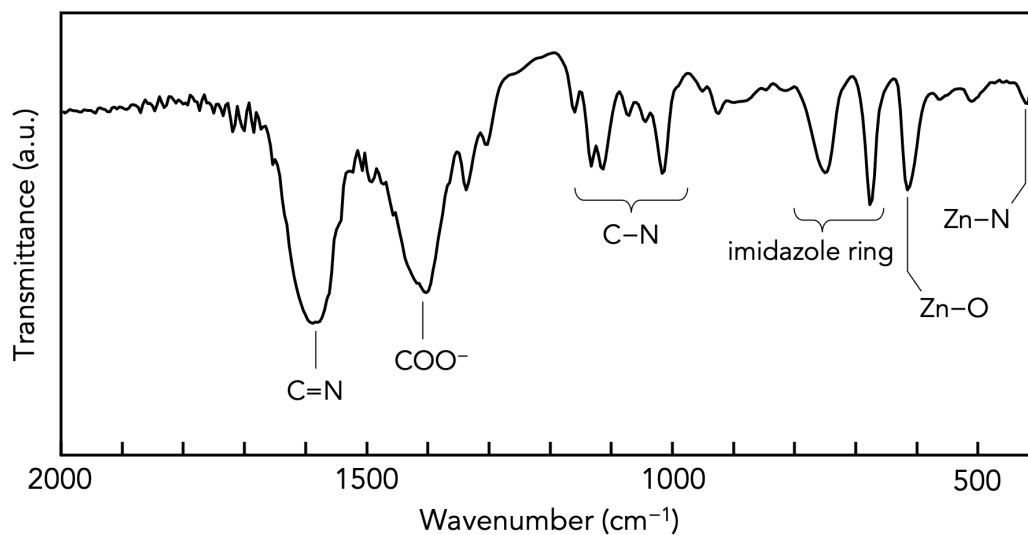


Fig. S2 FTIR spectrum of the *amp*-Zn-Hmim precursor deposited on a Si substrate for measurement.

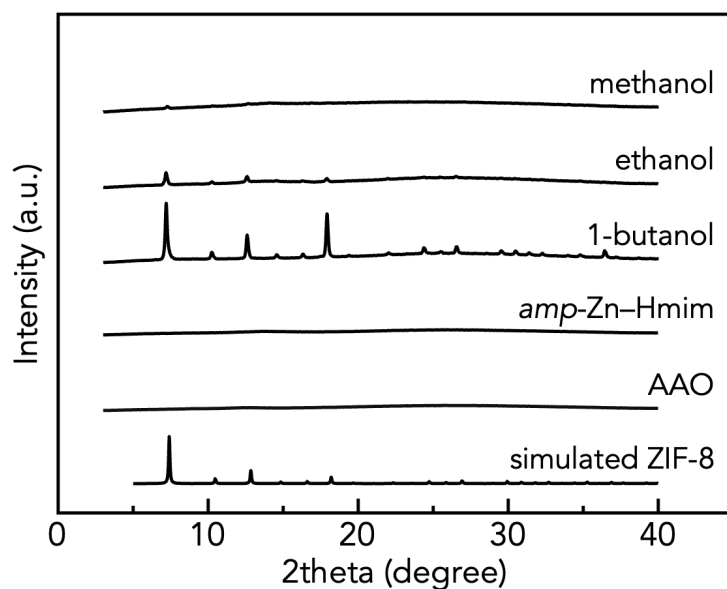


Fig. S3 XRD patterns of *amp-Zn-Hmim* membranes after vapor treatment with methanol, ethanol, and 1-butanol for 2 h.

Methanol treatment did not induce noticeable crystallization within 2 h, while the ethanol-treated membrane exhibited only weak diffraction peaks corresponding to ZIF-8. In contrast, 1-butanol treatment resulted in clear and well-defined crystalline transformation.

The distinct behavior of 1-butanol is likely related to a balanced combination of vapor pressure, molecular size, and hydrogen-bonding ability. Methanol, owing to its high vapor pressure and small molecular size, may diffuse rapidly into the amorphous layer but provide insufficient residence time and local interaction to promote framework rearrangement. Ethanol exhibits limited crystallization behavior, suggesting partial effectiveness under the present conditions. In contrast, 1-butanol, with its lower vapor pressure and moderate steric bulk, may generate a more favorable transient solvation environment within the amorphous network, facilitating structural reorganization into crystalline ZIF-8. These observations suggest that a balanced solvent-framework interaction is critical for inducing the amorphous-to-crystalline transformation.

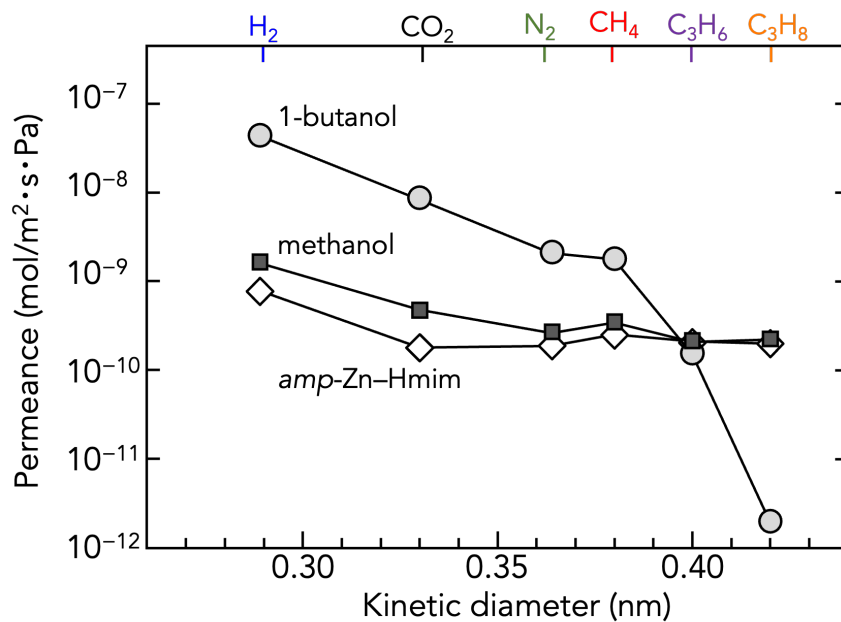


Fig. S4 Single-gas permeance of the *amp*-Zn-Hmim membrane (0 h) and the membranes after 2 h vapor treatment with methanol and 1-butanol.

Gas permeation data for the methanol-treated membrane show performance comparable to that of the original amorphous membrane, confirming the absence of effective structural conversion.

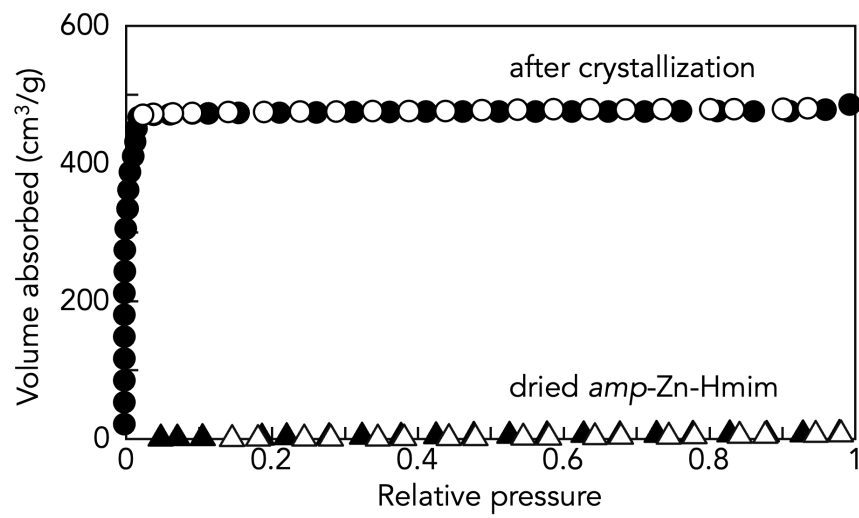


Fig. S5 N₂ adsorption and desorption isotherms of dried *amp*-Zn-Hmim before and after crystallization.

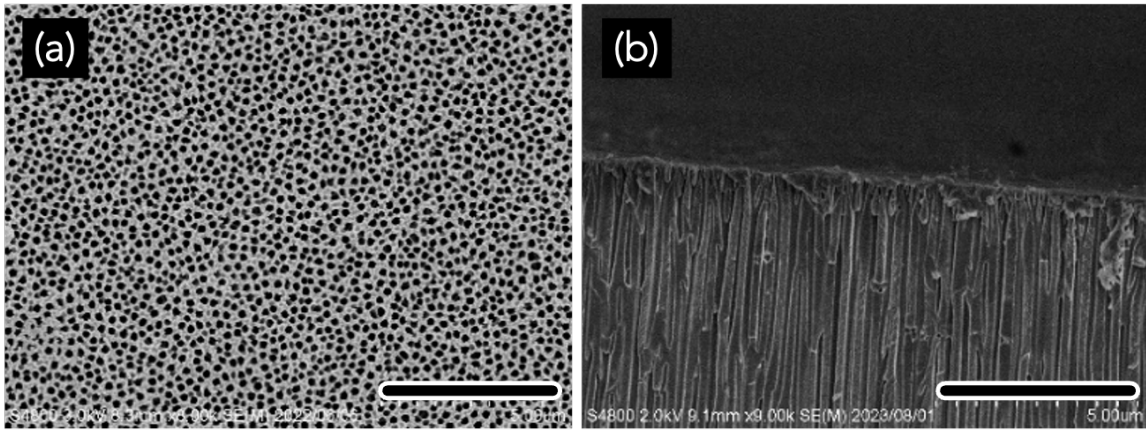


Fig. S6 FESM images of the pristine AAO substrate: (a, b) surface view and (b) cross-sectional view. Scale bar: 5 μm .

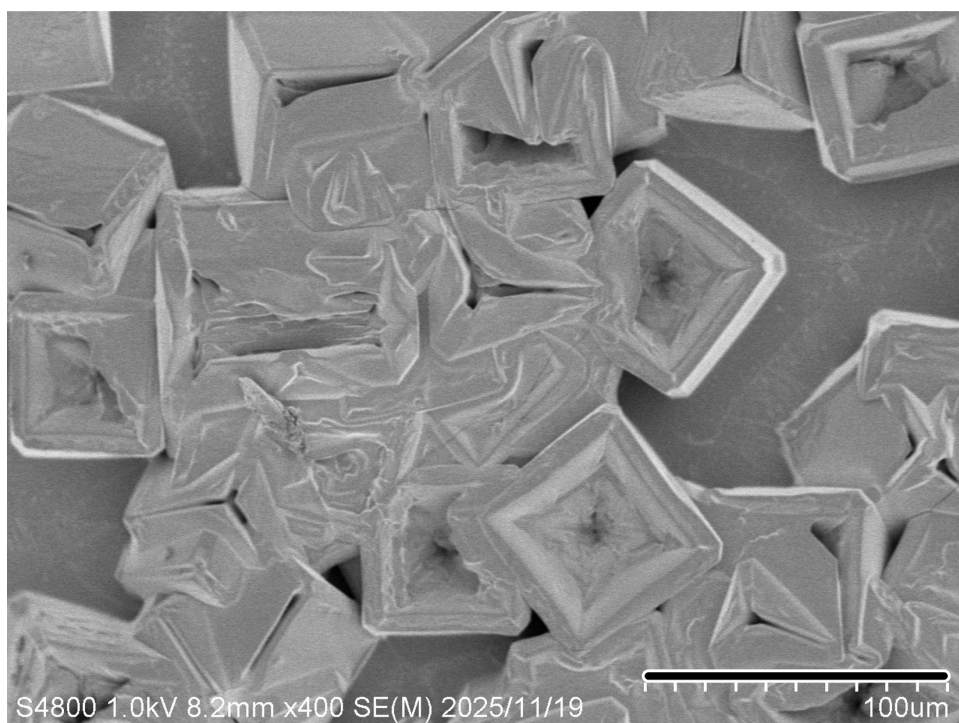


Fig. S7 FESEM image of a deliberately thickened *amp*-Zn-Hmim-derived sample after 1-butanol vapor treatment, showing well-developed individual ZIF-8 crystals. Large concave features are observed within single crystals, which may be associated with local precursor depletion during crystal growth.

To gain further insight into the crystallization process, FESEM observations were conducted on a deliberately thickened sample, where individual ZIF-8 crystals could be clearly resolved. Notably, large concave depressions were observed within single crystals, suggesting local precursor depletion and network reconstruction during crystal growth. These features support the proposed mechanism of crystallization under constrained precursor supply.

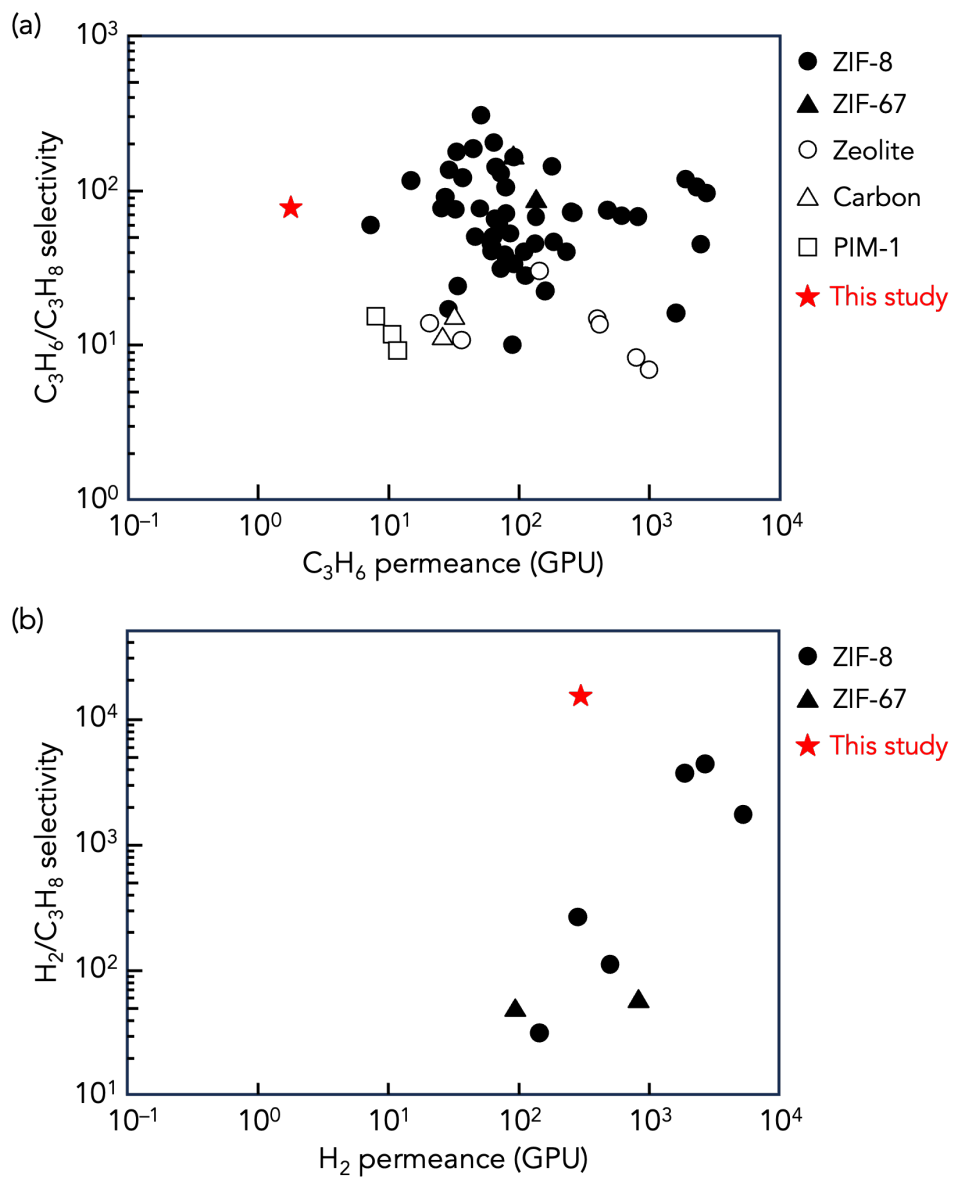


Fig. S8 Comparison of the gas permeation characteristics of the reference separation membranes.